Dynamic Imaging of Lymphatic Vessels and Lymph Nodes Using a Bimodal Nanoparticulate Contrast Agent

RAWAD MOUNZER, M.D.,[1] PAVEL SHKARIN, Ph.D.,[2,3]
XENOPHON PAPADEMETRIS, Ph.D.,[2,3] TODD CONSTABLE, Ph.D.,[2,3]
NANCY H. RUDDLE, Ph.D.,[1,4] and TAREK M. FAHMY, Ph.D.[3]

ABSTRACT

Background: Evaluation of lymphedema and lymph node metastasis in humans has relied primarily on invasive or radioactive modalities. While noninvasive technologies such as magnetic resonance imaging (MRI) offer the potential for true three-dimensional imaging of lymphatic structures, invasive modalities, such as optical fluorescence microscopy, provide higher resolution and clearer delineation of both lymph nodes and lymphatic vessels. Thus, contrast agents that image lymphatic vessels and lymph nodes by both fluorescence and MRI may further enhance our understanding of the structure and function of the lymphatic system. Recent applications of bimodal (fluorescence and MR) contrast agents in mice have not achieved clear visualization of lymphatic vessels and nodes. Here the authors describe the development of a nanoparticulate contrast agent that is taken up by lymphatic vessels to draining lymph nodes and detected by both modalities.

Methods: A unique nanoparticulate contrast agent composed of a polyamidoamine dendrimer core conjugated to paramagnetic contrast agents and fluorescent probes was synthesized. Anesthetized mice were injected with the nanoparticulates in the hind footpads and imaged by MR and fluorescence microscopy. High resolution MR and fluorescence images were obtained and compared to traditional techniques for lymphatic visualization using Evans blue dye.

Results: Lymph nodes and lymphatic vessels were clearly observed by both MRI and fluorescence microscopy using the bimodal nanoparticulate contrast agent. Characteristic tail lymphatics were also visualized by both modalities. Contrast imaging yielded a higher resolution than the traditional method employing Evans blue dye. MR data correlated with fluorescence and Evans blue dye imaging.

Conclusion: A bimodal nanoparticulate contrast agent facilitates the visualization of lymphatic vessels and lymph nodes by both fluorescence microscopy and MRI with strong correlation between the two modalities. This agent may translate to applications such as the assessment of malignancy and lymphedema in humans and the evaluation of lymphatic vessel function and morphology in animal models.

INTRODUCTION

VISUALIZATION OF THE LYMPHATIC SYSTEM plays a significant role in assessing patients with various malignancies and lymphedema.[1,2] Current patient imaging modalities, such as lymphography and lymphoscintigraphy, are invasive and may expose patients and physicians to radiation.[3,4] In particular, lymphography, in addition to being technically difficult, causes significant patient discomfort and may lead to potential complications such as reaction to the dye, pulmonary emboli, and wound infections.[3,5] In animal models, lymphography has been predominantly limited to the use of Evans blue dye[7] and fluorescently labeled dextrans.[8] Lymphoscintigraphy, which is traditionally used to localize sentinel lymph nodes, has low temporal and spatial resolution and fails to adequately demonstrate the direct connection of lymphatic vessels to the associated nodes. Moreover, vascular spillage of the radiotracer may lead to the labeling of non-sentinel lymph nodes.[4,6]

As a result of these limitations and combined with the promise of magnetic resonance imaging (MRI) for the noninvasive visualization of both lymphatic vessel structure and lymph nodes, various contrast agents that enhance the MR signal *in vivo* have been introduced.[9–13] The design of these agents needs to take into account current understanding of interstitial transport mechanics and function of lymphatic vessels.[1,14] Thus, to facilitate noninvasive visualization of both lymphatic vessels and lymph nodes,[11,13] an ideal contrast agent needs to be sufficiently large to prevent leakage into blood vessels. At the same time, the agent needs to be sufficiently small for rapid transport through the lymphatics during the time course of the imaging experiment.

Despite significant advances in nanoparticulate-based systems, clear visualization of both lymphatic vessels and lymph nodes by both MRI and fluorescence in living animals has been limited.[13] Here we describe the development and demonstration of a bimodal nanoparticulate contrast agent which has been optimized for fluorescent microscopy and MRI. Upon subcutaneous administration, the nanoparticles are quickly (within minutes) taken up by the lymphatic vessels to the draining nodes and are detected by MRI. Computational processing of our images with in-house developed software (Yale Bioimage Suite medical image analysis software) allowed further refinement and realization of high resolution images. This bimodal agent thus offers a noninvasive, sensitive, nonisotopic, and dynamic means of evaluating the lymphatic vasculature and nodes, potentially enabling further evaluation of animal models of lymphatic system pathology and extrapolation to clinical settings.

MATERIALS AND METHODS

All experiments were conducted on female C57BL/6J mice (8–12 weeks old) obtained from the Jackson Laboratory (Bar Harbor, Maine) and in accordance with established animal protocols maintained and approved by the Institutional Animal Care and Use Committee at Yale University and Yale School of Medicine.

Synthesis and characterization of the nanoparticulate contrast agent

We selected polyamidoamine dendrimers (PAMAM) (generation 6 (G6) diameter = 7.2 nm, 256 theoretical functional groups) as the foundation for the design of the bimodal imaging construct because of their demonstrated potential as nanoscopic polymers for conjugation to a variety of agents.[15,16] The design criteria necessitated that the final size of these particles, following attachment of imaging agents, be large enough to prevent their leakage into blood capillaries. Additionally, the particles could not be larger than 30–50 nm as that would reduce their trafficking from the injection site (on the order of days), thus slowing lymphatic drainage and negatively impacting the utility of the imaging procedure.[3] These two requirements; the size of the agent for exclusive and rapid uptake by the lymphatic system combined with the need to attain high paramagnetic relaxivity for MR, dictated our design of the bimodal nanoparticle.

The PAMAM core was conjugated with SCN-DTPA, NHS-PEG5000-FITC and NHS-PEG3400-OH in a molar ratio of (40:3:7) using

a single reaction step (Fig. 1A). Polyethylene glycol (PEG) was then tethered to the dendrimer core for several reasons: first, PEG is a linear polymer that imparts flexibility and colloidal stability to the attached PAMAM core while also drawing water into the construct volume. This feature is useful for maximizing T1 contrast that depends on water relaxation. Second, by stabilizing the surface with PEG, useful properties such as enhanced solubility, biocompatibility, lower immunogenicity, reduced toxicity, and desirable pharmacokinetics can be introduced into the construct.[17] These critical properties allow for safe and efficient use of this technology *in vivo*.

Following dialysis of the construct, a 100-fold molar excess of $GdCl_3.6H20$ was added and allowed to equilibrate for 48 h at room temperature with the construct; this was followed by a second round of dialysis to remove unchelated gadolinium III. The final product contained up to 23 moles of gadolinium per mole of dendrimer assessed by a colorimetric Arsenazo III assay (Fig. 1B) and showed an enhanced T1 relaxation compared to free Gd/DTPA at the same concentration (Fig. 1C). FT-IR and NMR spectra of the conjugate confirmed the formation of amide conjugates, and fluorescence spectroscopy (excitation 488 nm and emission at 520 nm) confirmed the presence of fluorescein. Final conjugate size was assessed by dynamic light scattering and showed that constructs were distributed in size with a mean diameter of 30 ± 10 nm.

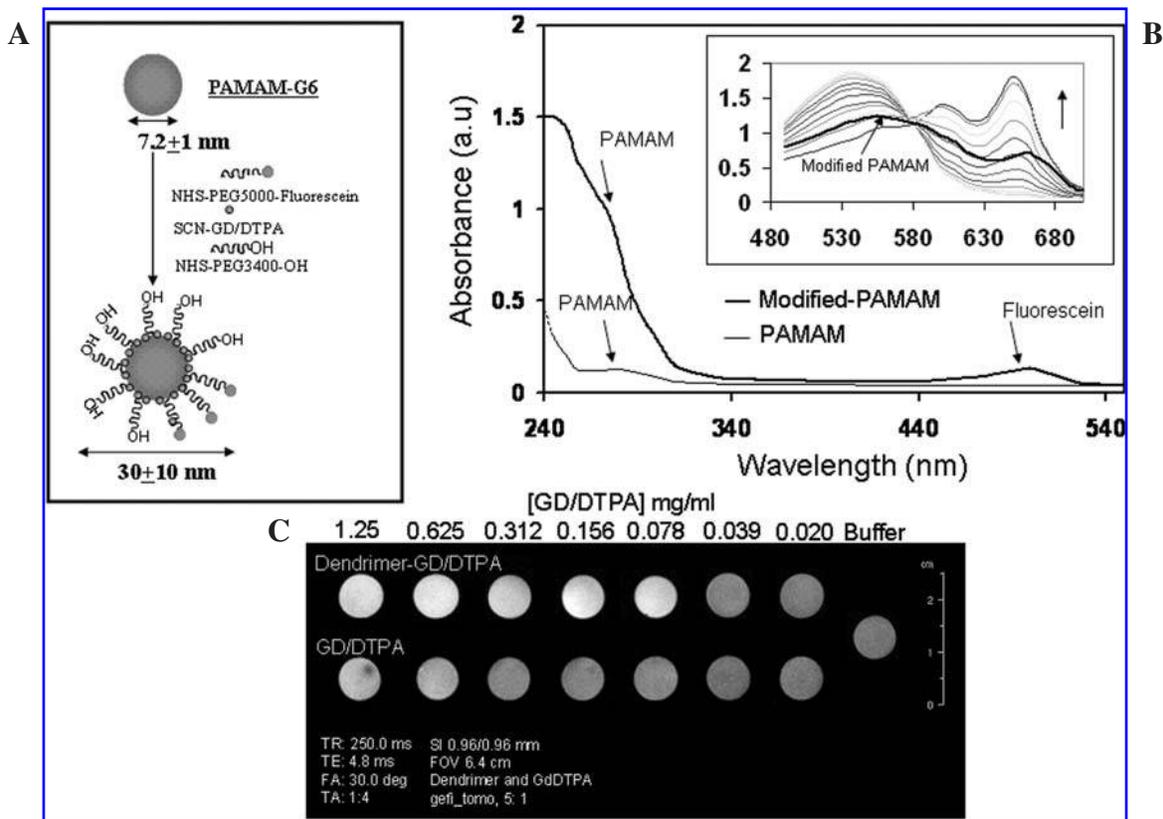The size of the constructs was measured by dynamic light scattering (DLS). The instrument

FIG. 1. Synthesis and characterization of the dendrimer-based bimodal contrast agent. (**A**) Schematic outline of polyamidoamine dendrimer and reaction conditions yielding the bimodal contrast agent. (**B**) UV-VIS characterization of the modified PAMAM dendrimer compared to unmodified PAMAM. Peaks at 278 nm and 488 nm are characteristic of PAMAM and fluorescein, respectively. *Inset:* Characterization of PAMAM GD/DTPA (*solid black line*) compared to increasing concentrations of free GD/DTPA (*direction of the black arrow*) using a colorimetric assay based on an absorbance increase of Aresnazo III at 650 nm and decrease at 548 nm in the presence of GD/DTPA. Aresnazo III solution: (15 m*M* Arsenazo III, 0.1 *M* nitric acid, 0.01 *M* urea). *Solid black line* indicates approximately 23 moles of GD/TPA bound per mole of dendrimer. (**C**) T1 weighted relaxation of dendrimer–GD/DTPA compared to free GD/DTPA.

consisted of a diode pumped laser (Verdi V-2/V-5, Coherent) operating at 532 nm, an ALV-SP S/N 30 goniometer (ALV-GmbH, Langen, Germany) with index matching vat filled with doubly filtered (0.1 mm) toluene, and an ALV-500 correlator. Low concentrations of constructs (<5 ug/mL) were pipetted into a cleaned borosilicate culture tube before measuring the intensity of the auto-correlation function at a 90° scattering angle. The hydrodynamic radius, RH, was determined by nonlinear least squares fitting (ALV software) of the resulting second order cumulants.

Magnetic resonance imaging

MRI of the mice was performed using a 4.7T Bruker scanner operating at 4T. The mice that underwent MR imaging were anesthetized with 250 μL i.p. injections of ketamine (10 mg/mL) and xylazine (1 mg/mL) and examined for pain response to toe pinch to ensure adequate anesthesia prior to contrast injections. The tip of a 30 G needle was broken off the plastic base and fitted into a polyethylene tube with 28 mm I.D. (BD Biosciences, Sparks, MD). The tubing was also fitted into another 30 G needle attached to a 1 mL syringe containing contrast at 15 mg/mL in PBS. The anesthetized mouse was secured onto a plexiglass custom-constructed coil holder with the imaging area of interest centered in the coil. The needle was inserted subcutaneously into the hind footpad and secured using tape. The animals were imaged prior to contrast injection to generate a control image. Fifty μL of contrast was then injected while the animal remained secured within the magnet. This procedure was repeated with the needle fixed subcutaneously in the tail of anesthetized mice 3 cm proximal to the tip.

Injection was followed by dynamic acquisitions using a 4T Bruker AVANCE system equipped with 5.4 KHz/cm, 150 ms rise time gradients. A series of imaging sessions were then performed to detect the contrast within the lymphatic vessels and lymph nodes. This remote injection technique facilitated registration and subsequent processing of images obtained both before and after injections. All images were obtained using a T1-weighted 3D fast gradient echo (GEFI) pulse sequence.

MRI image processing

Contrast uptake was quantified by subtraction of the reference image (before injection) from the target image (after agent injection). Prior to the subtraction, the images were registered to account for any movement between scans and intensity normalized to correct for the different dynamic ranges in the images. The intensity normalization was based on a k-means segmentation of the image to identify the histogram peak corresponding to soft tissue (muscle) which is assumed to be unchanged between the two images and by scaling the reference image to have the same soft-tissue mean as the reference image.[18] All image analysis was performed using the Yale BioImage Suite medical image analysis software package. All difference MR images were overlaid on the anatomical control images.

Optical microscopy: fluorescence and Evans Blue dye imaging

The bimodal nanoparticulate contrast agent was diluted to a concentration of 15 mg/mL in PBS. Fifty μL of the dendrimer was injected subcutaneously into each of the hind footpads of the animals using a 1 mL syringe and a 30 G needle. Mice were sacrificed using a CO_2 chamber 30 min following injection. The popliteal lymph node was exposed by means of a vertical skin incision over the calf and retraction of the skin. The inguinal lymph nodes were exposed by means of a vertical midline skin incision over the abdomen and thorax and retraction of the skin. The para-aortic lymph nodes were exposed by a midline incision of the abdomen and retraction of the intestines and mesentery revealing the bifurcation of the aorta. These nodes and associated lymphatic vessels were all visualized using a Zeiss Lumar® fluorescent dissecting microscope. Absence of detectable fluorescence in the tissues and vasculature of these animals confirmed full uptake of contrast agent in the lymphatic vessels and lymph nodes.

To visualize the lymphatic vessels in the tail, the mice were anesthetized as above, and 10 μL of contrast at a concentration of 15 mg/mL was injected subcutaneously in the tail 3 cm proximal to the tip. Images were acquired as dis-
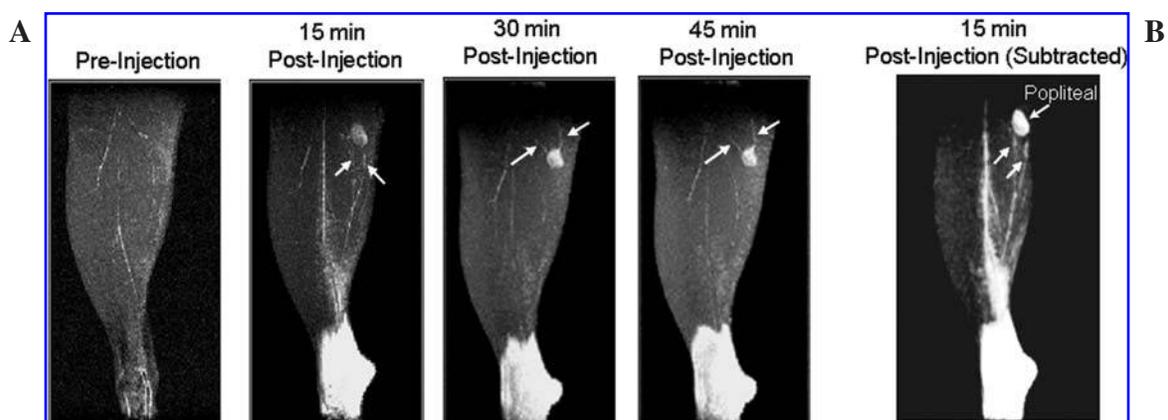
FIG. 2. Kinetics of bimodal agent uptake into lymphatic vessels and lymph nodes. (**A**) Maximum intensity (MRI) projections of the hind limb pre- and postinjection (50 μL of a 15 mg/mL solution in phosphate-buffered saline injected subcutaneously in the hind limb) using a hind limb volume coil. *Arrows* point to afferent vessels (15 min postinjection) and efferent vessels (30 and 45 min postinjection). (**B**) Subtracted image at 15 min postinjection clearly reveals lymphatic vessels (*white arrows*) coursing through the hind limb and accumulating in the popliteal lymph node. Animated three-dimensional view of contrast uptake in the hind limb is shown in supplementary movie online.

cussed above, 10 min following injection. Evans blue dye was injected in a similar manner and lymph nodes were exposed as described above and imaged using a Zeiss Stemi® 2000-C dissecting microscope.

RESULTS

MRI detection of lymphatic vessels and lymph nodes

Our initial studies focused on demonstrating the utility of the nanoparticulate contrast agent in highlighting lymphatic vessels draining to lymph nodes in the hind limb of living mice. We observed that 15 min after subcutaneous injection into the hind footpad, the agent readily entered lymphatic vessels of the hind limb that drain towards the popliteal lymph node (Fig. 2A). Two distinct afferent lymphatic vessels coursing towards the popliteal lymph node could be seen in subtracted MR images of the hind limb following contrast administration and are clearly distinct after subtraction of the pre-injection image (Fig. 2B and supplementary movie online). We also observed contrast enhancement in efferent vessels at later times following injection (Fig. 2A). Strikingly, accumulation of the contrast agent in the popliteal node and contrast in efferent vessels was observed for over 45 min postinjection in sharp
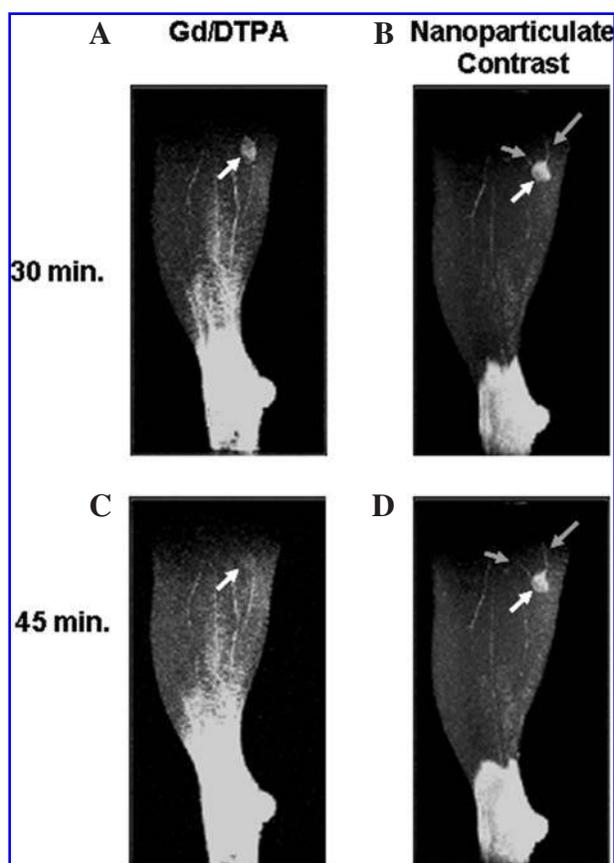

FIG. 3. MRI of hind limb 30 min and 45 min postinjection of free (**A**, **C**) Gd/DTPA and (**B**, **D**) dendrimer in the foot pad. Persistent accumulation of dendrimer contrast in the popliteal lymph node (*white arrow*) and appearance of efferent lymphatic vessels exiting the node (*grey arrows*).
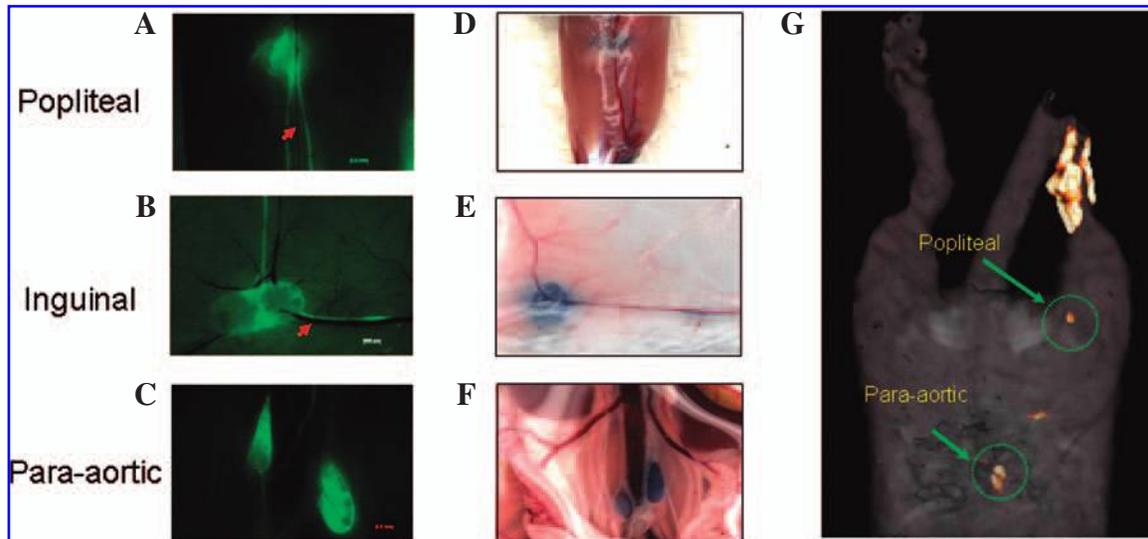
FIG. 4. Bimodal agent contrast allows accurate visualization of lymphatic vessels and lymph nodes by MRI and fluorescence imaging. (**A–C**) Fluorescence microscopy visualization of lymph node agent uptake in (**A**) popliteal, (**B**) inguinal and (**C**) para-aortic lymph nodes. Excitation at 470 nm and emission at 520 nm. No contrast agent is detected in adjacent blood vessels (*red arrows*). Scale bars are 0.5 mm. (**D–F**) Evans blue dye visualization of the same lymph nodes as in (**A–C**). Dye injected subcutaneously (30 μL, 30 min) into the hind footpads. (**G**) Subtracted whole body MR imaging 30 min postinjection. Starting from the tail end and indicated by *green arrows* are the popliteal and para-aortic lymph nodes, respectively. Pre- and postimages acquired with a 4 cm diameter whole body bird cage coil.

contrast to the disappearance of an equivalent dose of free gadolinium/DTPA (Fig. 3).

Verification of MR images by fluorescence and Evans Blue dye lymphography

MR images obtained with the bimodal agent were then compared to high resolution fluorescence microscopy of lymphatic uptake. Fluorescence microscopy experiments were performed using the same procedures as the MRI experiments. Mice were euthanized 30 min following injection of the contrast agent and the popliteal, inguinal, and para-aortic lymph nodes were exposed and visualized using high resolution stereo-fluorescence microscopy (Figs. 4A–4C). Fluorescence imaging of the above mentioned lymph nodes showed high concordance with the lymphatic vessels and nodes visible in the subtracted MR images (Fig. 4G) yielding nearly identical images by both modalities. Additionally, the two afferent lymphatic vessels seen by MRI draining into the popliteal lymph node (Fig. 2B) were also seen by fluorescence microscopy (Fig. 4A). Lymph nodes and associated lymphatic vessels were more clearly visible by fluorescence microscopy compared to standard lymphography

using Evans blue dye (Figs. 4D–4F). Additionally, the nanoparticulate agent, in sharp contrast to the Evans blue dye, showed a more defined distribution within the node. A more prominent signal was detected in the lymph node medulla and subcapsular sinus, most evident in the inguinal and para-aortic lymph nodes (Figs. 4B and 4C). This may be attributed to the fact that Evans blue dye is conjugated to plasma proteins,[19] and that lymph nodes are capable of modifying lymph flow and protein concentrations by means of their specialized blood and lymphatic vasculature.[20] Thus, plasma proteins may extravasate from within the lymph node vasculature, causing dye to accumulate within the entire node. The nanoparticulate contrast however, appears to be more restricted to the medullary and marginal sinuses within the lymph node medulla and subcapsular region.

Examination of tail lymphatics using bimodal nanoparticulate contrast

The efficacy of the bimodal reagent in elucidating the well-studied, unique hexagonal network of lymphatic vessels in the mouse tail[21] was then evaluated. Anesthetized mice were
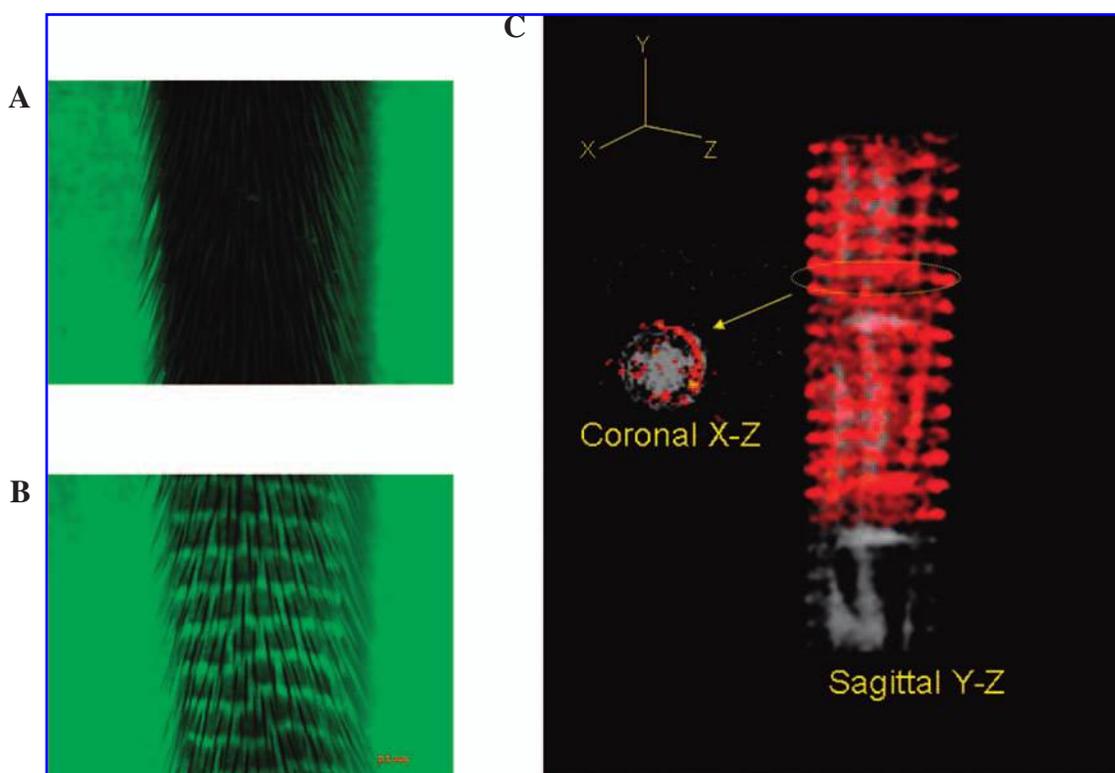
FIG. 5. Characteristic honeycomb network of lymphatic vessels in the tail detected using the bimodal contrast agent. (**A**) Pre-injection of contrast agent. Subcutaneous tail injection reveals the distinct lymphatic vasculature of the tail by both (**B**) fluorescence imaging and (**C**) MR imaging. Sagittal and coronal sections of pre-and 15 min postinjection subtracted images show localization of tail lymphatics to the peripheral surface of the tail.

injected subcutaneously proximal to the tip of the tail with the agent, and tail lymphatics were visualized in living animals by both fluorescence microscopy (Figs. 5A and 5B) and MRI (Fig. 5C). Both modalities produced similar images revealing the honeycombed lymphatic vessel network in the tail. Moreover, MR revealed the preferential surface localization of these lymphatic structures highlighting the utility of the agent in discerning detailed three-dimensional lymphatic distribution.

CONCLUSION

Technology for noninvasive imaging of lymphatic vessels and lymph nodes has been limited by the signal-to-noise ratio and resolution that can be achieved. Several modalities have been proposed to address this issue focusing on the unique ability of nanoparticulates to couple to a high density of paramagnetic chelates, hence enhancing relaxivity. However,

these limitations have not been completely overcome due to a variety of factors including optimal contrast agent design, acquisition methods, and postacquisition image processing. In this report, we have incorporated all of these factors and demonstrated the utility of a new nanoscopic agent for high resolution imaging of the lymphatic system. The unique combination of highly sensitive fluorescence lymphography and superior spatial resolution achieved by noninvasive MR yields an approach that promises wide utility in basic science, with potential clinical applications for lymphatic visualization and serial assessment of patients with lymphedema or metastatic disease.

ACKNOWLEDGMENTS

01. X Papademetris, M Jackowski, N Rajeevan, RT Constable, and LH Staib. BioImage Suite: An integrated medical image analysis suite, Section of Bioimaging Sciences, Dept. of Diagnostic Radiology, Yale School of Medicine, <www.bioimagesuite.org>.

REFERENCES

1. Swartz MA. The physiology of the lymphatic system. Adv Drug Deliv Rev 2001;50:3–20.
2. Swartz MA, Skobe M. Lymphatic function, lymphangiogenesis, and cancer metastasis. Microsc Res Tech 2001;55:92–99.
3. Moghimi SM, Bonnemain B. Subcutaneous and intravenous delivery of diagnostic agents to the lymphatic system: applications in lymphoscintigraphy and indirect lymphography. Adv Drug Deliv Rev 1999;37:295–312.
4. Suga K, Yuan Y, Ogasawara N, Okada M, Matsunaga N. Visualization of normal and interrupted lymphatic drainage in dog legs with interstitial MR lymphography using an extracellular MR contrast agent, gadopentetate dimeglumine. Invest Radiol 2003;38:349–357.
5. Ruehm SG, Schroeder T, Debatin JF. Interstitial MR lymphography with gadoterate meglumine: initial experience in humans. Radiology 2001;220:816–221.
6. Suga K, Yuan Y, Ogasawara N, Okada M, Matsunaga N. Localization of breast sentinel lymph nodes by MR lymphography with a conventional gadolinium contrast agent. Preliminary observations in dogs and humans. Acta Radiol 2003;44:35–42.
7. Liao S, Ruddle NH. Synchrony of high endothelial venules and lymphatic vessels revealed by immunization. J Immunol 2006;177:3369–3379.
8. Reddy ST, Berk DA, Jain RK, Swartz MA. A sensitive in vivo model for quantifying interstitial convective transport of injected macromolecules and nanoparticles. J Appl Physiol 2006;101:1162–1169.
9. Hama Y, Bernardo M, Regino CA, Koyama Y, Brechbiel MW, Krishna MC, Choyke PL, Kobayashi H. MR lymphangiography using dendrimer-based contrast agents: A comparison at 1.5T and 3.0T. Magn Reson Med 2007;57:431–436.
10. Kobayashi H, Brechbiel MW. Dendrimer-based macromolecular MRI contrast agents: characteristics and application. Mol Imaging 2003;2:1–10.
11. Kobayashi H, Brechbiel MW. Dendrimer-based nano-sized MRI contrast agents. Curr Pharm Biotechnol 2004;5:539–549.
12. Rety F, Clement O, Slauve N, Cuenod CA, Carnot F, SIch M, Buisine A, Frija G. MR lymphography using iron oxide nanoparticles in rats: pharmacokinetics in the lymphatic system after intravenous injection. J Magn Reson Imaging 2000;12:734–739.
13. Talanov VS, Regino CA, Kobayashi H, Bernardo M, Choyke PL, Brechbiel NW. Dendrimer-based nanoprobe for dual modality magnetic resonance and fluorescence imaging. Nano Lett 2006;6:1459–1463.
14. Skobe M, Detmar M. Structure, function, and molecular control of the skin lymphatic system. J Investig Dermatol Symp Proc 2000;5:14–19.
15. Esfand R, Tomalia DA. Poly(amidoamine) (PAMAM) dendrimers: from biomimicry to drug delivery and biomedical applications. Drug Discov Today 2001;6:427–436.
16. Frechet JM. Functional polymers and dendrimers: reactivity, molecular architecture, and interfacial energy. Science 1994;263:1710–1715.
17. Katre NV. The conjugation of proteins with polyethylene glycol and other polymers. Adv Drug Deliv Rev 1993;10:91–114.
18. Studholme C, Hill DL, Hawkes DJ. Automated three-dimensional registration of magnetic resonance and positron emission tomography brain images by multiresolution optimization of voxel similarity measures. Med Phys 1997;24:25–35.
19. Maron MB. Modification of lymph during passage through the lymph node: effect of histamine. Am J Physiol 1983;245:H553–H559.
20. Adair TH, Moffatt DS, Paulsen AW, Guyton AC. Quantitation of changes in lymph protein concentration during lymph node transit. Am J Physiol 1982;243:H351–H359.
21. Swartz MA, Kaipainen A, Netti PA, Brekken C, Boucher Y, Grodzinsky AJ, and Jain RK. Mechanics of interstitial-lymphatic fluid transport: theoretical foundation and experimental validation. J Biomech 1999;32:1297–1307.

Address reprint requests to:
Tarek M. Fahmy, Ph.D.
Department of Biomedical Engineering
P.O.Box 208284
Yale University
New Haven CT 06520

E-mail: tarek.fahmy@yale.edu